Article:
Deastra, P., Wagg, D.J., Sims, N.D. et al. (2023) Experimental shake table validation of damping behaviour in inerter-based dampers. Bulletin of Earthquake Engineering, 21 (3). pp. 1389-1409. ISSN: 1570-761X

https://doi.org/10.1007/s10518-022-01376-1

Bulletin of Earthquake Engineering manuscript No.
(will be inserted by the editor)

Experimental shake table validation of damping behaviour in inerter-based dampers

Predaricka Deastra · David J. Wagg · Neil D. Sims · Robin S. Mills

Received: date / Accepted: date

Abstract Inerter-based-dampers have received substantial interest from the earthquake engineering community in the last two decades. These typically consist of an inerter, a linear spring and a viscous damper arranged into various possible configurations. In this paper, for the first time, experimental results are presented from shake table tests on a scaled three-storey structure with an inerter-based damper included, in order to suppress vibration amplitudes at the resonant frequencies. In particular two types of device are used to demonstrate the differences between using viscous and hysteretic damping in the inerter-based device. The two different types of experimental dampers were manufactured using eddy current dampers and gel damping material. The inerter was manufactured based on a flywheel design. The experimental results were compared with four analytical models tuned to suppress vibrations in the first resonance; namely the tuned-inerter-damper (TID), the tuned-inerter-hysteretic-damper (TIhD), the tuned-mass-damper-inerter (TMDI), and the tuned-mass-hysteretic-damper-inerter (TMhDI). These experimental results confirm the observations made from the models that the suppression of higher resonance peaks is significantly different between the viscous and hysteretic damped inerter-based-dampers. Consequently, it is recommended that future studies exploring the performance of inerter-based seismic mitigation systems pay close attention to the damping mechanisms that are prevalent within the structure.

Keywords inerter-based-damper · eddy current damper · linear hysteretic damping · shake-table experiment · gel damper · flywheel inerter

P. Deastra
Department of Civil Engineering, Islamic University of Indonesia, Kampus Terpadu UII, Jalan Kaliurang KM 14.5, Sleman, Yogyakarta, Indonesia.
E-mail: predaricka.deastra@uii.ac.id

D. J. Wagg · N. D. Sims · R. S. Mills
Department of Mechanical Engineering, The University of Sheffield, Mappin St, S1 3JD, Sheffield, United Kingdom.
E-mail: {david.wagg, n.sims, robin.mills}@sheffield.ac.uk

1 Introduction

Research relating to the inerter, which is a two-terminal device generating force proportional to the relative acceleration between its two terminals, for vibration suppression systems has achieved a significant amount of interest in the last two decades. The term 'inerter' was firstly introduced by Smith [1] in early 2000. However, the concept of an inerter had previously been patented by Okumura Atsushi in 1997 [2]. In order to realise the inerter concept, the three most common physical mechanisms that have been used are rack-and-pinion [1], ball-screw [3, 4], and fluid flow [5] — see recent review [6] and references therein. Numerous researchers have studied the use of the inerter for vibration control systems, particularly passive vibration control, by combining them with springs and dashpots in various configurations, in order to create inerter-based-dampers. Three types of inerter-based dampers that have received particular attention in the literature are the tuned-viscous-mass-damper (TVMD) [7], the tuned-inerter-damper (TID) [8], and the tuned-mass-damper-inerter (TMDI) [9].

The TVMD was firstly introduced by [7]. It consists of an inerter in parallel with a dashpot, then together these two elements are connected in series with a spring. The realisation of this device by [10] combines a viscous-mass-damper (VMD) and a chevron bracing. The VMD is a realisation of a parallel connected inerter and dashpot. The translational motion from the structure is converted to rotational motions of a flywheel and at the same time also generates viscous damping forces due to the fluid flow inside the VMD. A similar VMD concept realisation was also discussed in [11] where a helical fluid inerter was proposed as a parallel connected inerter-dashpot. To form a TVMD, this fluid inerter was connected to a chevron bracing providing the stiffness.

The TID concept was firstly introduced by [8]. Its configuration is similar to the tuned-mass-damper (TMD) but instead of a secondary mass element like the TMD, an inerter element is used instead. Another inerter-based damper found in the literature is the TMDI which is a TID with the addition of a secondary mass between the inerter and the parallel spring-dashpot. This secondary mass could be used to model the mass of the inerter or an additional mass element. The design and optimum tuning of the TMDI has been extensively discussed in the literature, see for example [9, 12–14] and references therein.

All these inerter-based devices have some potential advantages over the TMD because, as discussed in [8], they can be designed to have a very large mass ratio with a small actual mass. This is due to the fact that a large inerter constant (called the inertance) can be produced with a small gravitational inerter mass. For example, an inerter designed by [15] is capable of generating 75kg inertance while the actual mass of the inerter is only 2kg. Another potential advantage is that, unlike the TMD, the optimum location of the inerter-based device in a multi-storey building is between the first storey and the ground, saving space in the upper storeys [8]. However, for the purposes of this paper, the most significant advantage compared to the TMD is that inerter-based devices can reduce resonant amplitudes at all the resonance peaks of a multi-storey structure. This is in contrast to the TMD which can only mitigate the vibration amplitudes around a single resonance peak.

In civil engineering applications, inerter-based dampers have been studied for reducing structural response due to wind [16, 17] and seismic loadings [18–22].

Another interesting application of inerter-based devices in civil structures is as an earthquake protection device for base-isolated structures (BIS). This inerter-based-damper-BIS combined control strategy concept was proposed to solve two long-standing issues with a BIS: (1) they suffer from long period earthquakes due to resonance [23,24] (2) they require a large space on the isolation floor to accommodate the base-isolation displacement [25]. Some interesting examples of this combined control strategy can be found in [13,26–29].

Despite all of these promising applications of inerter-based-devices for reducing vibrations in building structures, there are currently only a very few practical implementations or experimental studies that have been carried out. The realization of the TMDI was firstly presented in [30]. Then in 2017, Gonzalez-Buelga, *et al.* [31] presented experimental results on a TID with nonlinearities. Recently, the first shake table experiment of a TMDI attached to a single degree-of-freedom (SDOF) structure was presented in [32] and [33]. To the best of the authors' knowledge there are no published shake table experimental results with a TID or TMDI that have been performed on a multi-storey structure. This paper is therefore the first to present shake table experiments of a multi-storey structure equipped with an inerter-based device.

It is important to note that the viscous damping element in the TID and TMDI models is an approximation to the real damping. This is often not physically realistic, and it is possible that the damping can exhibit linear hysteretic behaviour, particularly if a material damper is employed. The key modelling discrepancy occurs because the dissipated energy per cycle from viscous damping is frequency dependent. In contrast, most material damping is frequency independent [34]. As a result, for multi-degree-of-freedom structures that have multiple resonance peaks across a range of frequencies, there will be a difference in vibration suppression behaviour between these two different types of damper.

Two novel models have been proposed in [35] to capture this phenomenon, by introducing a hysteretic damper to give tuned-inerter-hysteretic-damper (TIhD) and tuned-mass-hysteretic-damper-inerter (TMhDI) models. Instead of using viscous damping, the damping in the TIhD and TMhDI is assumed to be coupled to the stiffness element modelled as a complex stiffness $k(1 + j\eta)$. The concept of complex stiffness was motivated by the fact that the energy loss per cycle in most materials is independent of excitation frequency and proportional to amplitude squared. This concept has been widely used in the literature. Although it is a non-causal model, it has been proven to be accurate if used appropriately [34,36].

In this paper a set of shake table experiments of a three-storey fixed base structure is presented. A hysteretic-inerter-based system was designed and installed between the first storey and the ground (shake table). It consists of two gel dampers connected in series to a flywheel inerter. Four analytical models are proposed to capture the structural performance: (1) TID; (2) TIhD; (3) TMDI; and (4) TMhDI. The obtained results from the shake table experiments are compared with the proposed models to find which model gives the best representation of the system.

For comparison, a set of shake table experiment was also performed on the same benchmark structure. But this time the gel dampers were replaced by eddy current (i.e., magnetic) dampers and springs. This arrangement realises the viscous-inerter-based device. The results were also compared with the four proposed models to verify which of them gives the best prediction to the experiments. The rationale of

these experiments is to show the difference between viscous and hysteretic damping when used in a real physical inerter-based system, especially the difference in the response amplitude around resonances at higher frequencies. The intention is to experimentally validate the results previously shown analytically in [35].

In Section 2 the three-storey steel structure is introduced, including the experimental test rig and the simplified mathematical model to be used. Then in Section 3 the design and specification of the experimental inerter and damper components is described. This is followed in Section 4 by the results from the shake table experiments. Conclusions are given in Section 6.

2 Three-storey steel structure

2.1 Structural system & mathematical model

The three-storey steel structure considered in this study is a 1:5 scaled model and is shown in Figure 1(a). The schematic diagram used to derive a simplified mathematical model is shown in Figure 1(b), where for now the structural damping has been neglected. The structural dimensions are shown in Figure 2. The structure is separated into three parts: bottom storey, $i = 1$; middle storey, $i = 2$; and top storey, $i = 3$. In this study, both hysteretic- and viscous-inerter-based systems will be designed and installed to the structure between the first storey and the ground (shake table).

The equations of motion of the 3-DOF structure equipped with an inerter-based system, as shown in Figure 1(b), can be written (in absolute coordinates) as

$$\begin{cases} (m_1 s^2 + k_{0,1} + k_{1,2})X_1 = k_{1,2}X_2 + k_{0,1}R + F_{1,0} \\ (m_2 s^2 + k_{1,2} + k_{2,3})X_i = k_{1,2}X_1 + k_{2,3}X_3 \\ (m_3 s^2 + k_{2,3})X_3 = k_{2,3}X_2 \end{cases} \tag{1}$$

where m_i and $k_{i-1,i}$, $i \in [1:3]$ represents the mass and stiffness between storeys $i-1$ and i; X_i represents the Laplace transform of the ith storey displacement, x_i, for $i = 0, 1, 2, 3$. Note that when $i = 0$, then $X_0 = R$ which represents the Laplace transform of the base displacement r (or x_0). The initial conditions are assumed to be zero, s represents the Laplace transform variable and $F_{1,0}$ denotes the force transferred to the structure by the proposed numerical models of the inerter-based device in Figure 4. $F_{1,0}$ for each of the models is given in Table 2 (defined in the Laplace domain).

2.2 Experimental test rig

A 1:5 scaled three-storey steel structure was installed on a multi-axis shaker table (MAST) system in a test chamber, as shown in Figure 1(a). The shake table dimension is 3m × 2m with a test frequency range of 3-70Hz. The MAST is connected to a reaction mass system consisting of a 300-tonne concrete block and springs. This system has natural frequency around 0.8-1.4Hz. Therefore, in order to avoid this resonance, no sinusoidal excitation test below 3Hz is allowed. In this

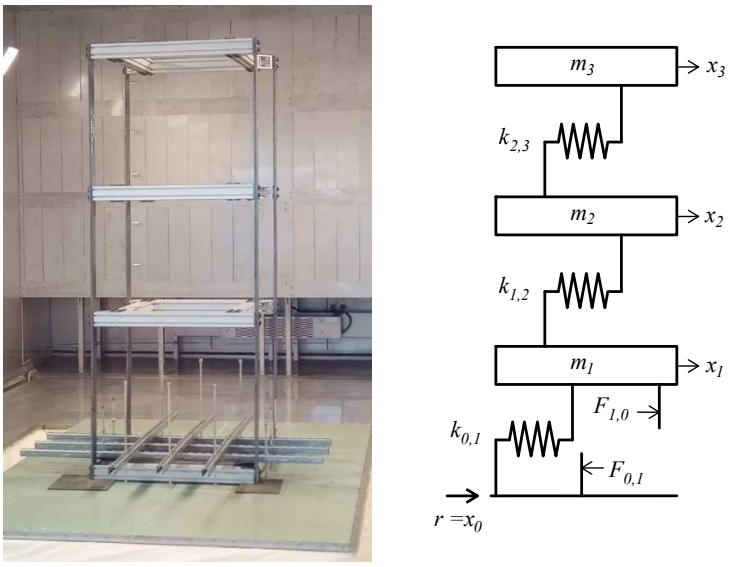

(a) (b)

Fig. 1 Three-storey steel structure showing: (a) a photograph of the test rig installed in a test chamber at the Laboratory for Verification and Validation, the University of Sheffield; (b) a schematic diagram of the three-storey structure used to derive a simplified mathematical model, where the structural damping has been neglected.

experiment, the minimum testing frequency was 3Hz, and the dimensions of the three-storey steel structure were designed accordingly.

The scaled three-storey steel structure is 900mm x 900mm in plan with a uniform inter-storey height of 780mm — see Figure 2. The cross section of the steel columns is 80mm × 12mm which makes the structure considerably more flexible in the direction of excitation (the direction from left hand side to right hand side of the chamber in Figure 1(a)) and therefore stiffer in the out-of-plane direction (the direction from outside to inside in Figure 1(a)). This design meant that the structure behaves more like a two-dimensional structure, and that three-dimensional effects (such as torsional modes) can be omitted from the current study. The ground floor of the structure is bolted on to the shake table, and this is where the support excitation to the structure is given.

The horizontal vibration response of the structure at each storey was measured using uniaxial accelerometers. The accelerometer type is PCB Piezotronics: 353B18 with a nominal sensitivity of 10mV/g. The horizontal vibration of the ground floor was also measured using a tri-axial accelerometer (only the horizontal axes are recorded). The accelerometer type is PCB Piezotronics: 356B21 with a nominal sensitivity of 10mV/g.

All accelerometer channels were sampled at 980Hz. For sinusoidal ground motions, the RMS of the signal was calculated at an update rate of 1Hz, and this was used to calculate the peak acceleration and displacement at each location on the shear building. At each frequency step, the building was left to settle for a period of time. This was manually determined by monitoring the stability of the RMS value. Measurements were taken when the RMS had visually stabilised. Measurements

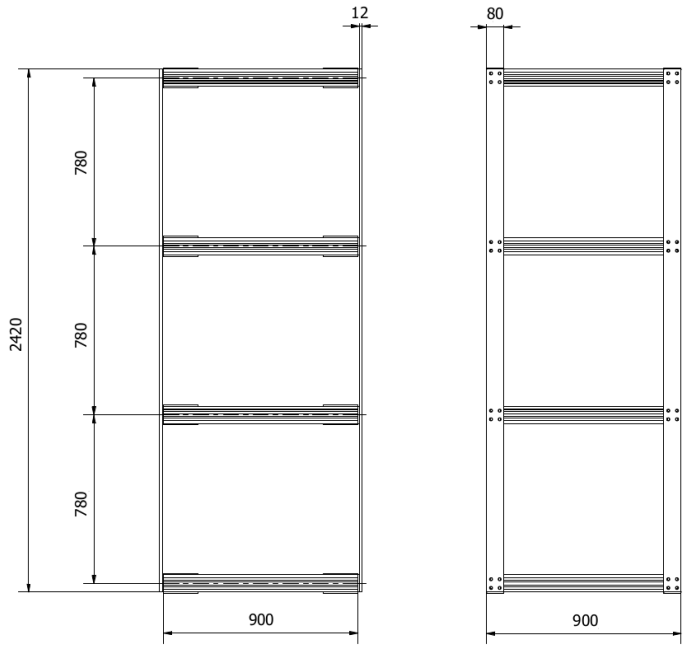

Fig. 2 The dimensions (in mm) of the three-storey steel structure.

were manually recorded at the ground level (using the MAST triaxial sensor), first storey level, second storey level and third storey level. At each frequency point, raw acceleration time domain data was captured for a period of 10 seconds.

Table 1 Properties of the structure

Storey/Mode	Mass (kg)	Stiffness (N/m)	Natural frequency (Hz)	Damping ratio, ζ
1	33.15	1.4048×10^5	5.3	0.46%
2	24.15	1.6858×10^5	15.1	0.19%
3	24.15	2.0792×10^5	24.2	0.17%

The first part of the experimental testing was to estimate the structural parameters. The structural mass of each storey was directly measured by firstly removing the masses from the structure. Some hammer tests were carried out on the uncontrolled structure ($F_{0,1} = F_{1,0} = 0$), and based on these results, initial estimates were made for the stiffness parameters of the simplified mathematical model. At the same time, estimates were made of the structural damping, based on the assumption of viscous damping. These initial results were verified using shake table tests performed on the uncontrolled structure. An example shake table test result is shown in Figure 3 in comparison to the output from the simplified mathematical model (with viscous damping terms added). The estimated structural parameters are very close to the experimental results. These parameters are given in Table 1.

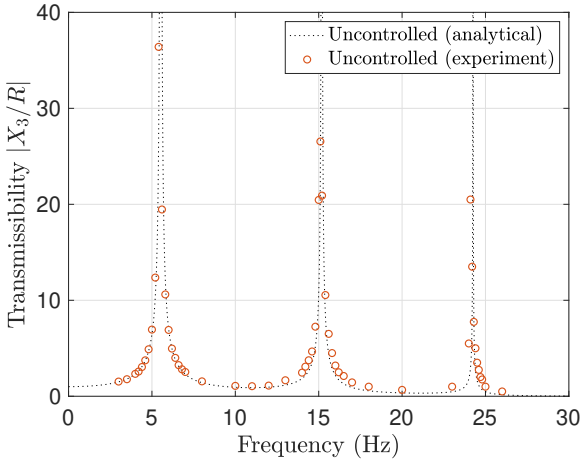

Fig. 3 Top floor transmissibility of the uncontrolled structure. The dotted line shows the output of the simplified analytical model (with added viscous damping) and the orange circles show experimentally recorded data points from the shake table testing.

2.3 Proposed analytical models for the inerter-based devices

The inerter-based systems were built and installed between the ground (shake table) and the first storey of the host structure. The hysteretic-inerter-based system was designed by connecting an inerter and material (e.g. hysteretic) damping element in series. The first terminal of the inerter was grounded and the other terminal was connected to the material damping element which was also attached to the first storey of the structure. In contrast, the viscous-inerter-based system was built by using electro-magnetic devices to create a viscous damping effect — a full description of the physical devices is given in Section 3.

In order to capture the behaviour of the physical devices, four analytical models are proposed. These have all been previously defined and studied in detail and are (i) the tuned-inerter-damper (TID) [8], (ii) the tuned-inerter-hysteretic-damper (TIhD) [35], (iii) the tuned-mass-damper-inerter (TMDI) [9], and (iv) the tuned-mass-hysteretic-damper-inerter (TMhDI) [35]. Schematic representations of these models are shown in Figure 4. The distinction between the four models has been extensively discussed in [35], but essentially the TID is the simplest model, and each of the other models includes additional components that are likely to more realistically capture the physics of the device in practice.

In Figure 4, $F_{1,0}$ and $F_{0,1}$ represent the force transferred to the structure by the four models given in Table 2 (defined in the Laplace domain), where b_d, m_d, and c_d are respectively the inertance, mass, and viscous damping coefficient of the device. In addition, k_d and η denote the stiffness and the loss factor, and $j = \sqrt{-1}$. Lastly, s_h is a constant with a unit of stiffness, such that $\eta = s_h/k_d$.

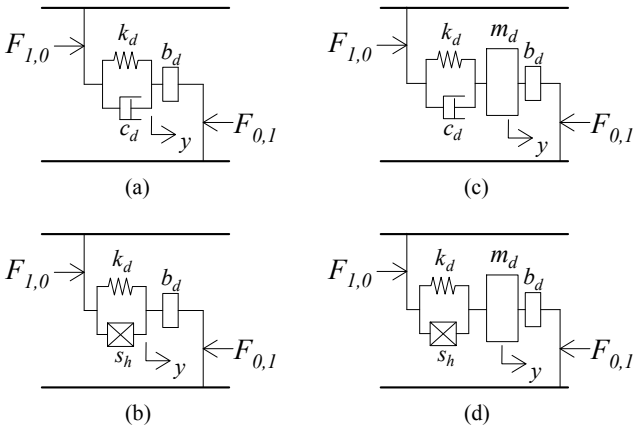

Fig. 4 Four models for the inerter-based devices, showing (a) TID (b) TIhD (c) TMDI (d) TMhDI. Device parameters are mass, m_d, stiffness, k_d, viscous damping, c_d, hysteretic damping constant, s_h, inertance, b_d. Note also that these models include an additional inertial degree-of-freedom that is denoted here using, y.

Table 2 Force transferred to the structure by the inerter damper in the Laplace domain [35]

Analytical model	$F_{1,0}$
TID	$\frac{b_d s^2(c_d s + k_d)}{b_d s^2 + c_d s + k_d}(R - X_1)$
TMDI	$\frac{b_d s^2(c_d s + k_d)}{(m_d + b_d)s^2 + c_d s + k_d}(R - X_1) - \frac{b_d s^2 m_d s^2}{(m_d + b_d)s^2 + c_d s + k_d}X_1$
TIhD	$\frac{b_d s^2(k_d(1 + j\eta))}{b_d s^2 + k_d(1 + j\eta)}(R - X_1)$
TMhDI	$\frac{b_d s^2(k_d(1 + j\eta))}{(m_d + b_d)s^2 + k_d(1 + j\eta)}(R - X_1) - \frac{b_d s^2 m_d s^2}{(m_d + b_d)s^2 + k_d(1 + j\eta)}X_1$

3 Design of the inerter and dampers

3.1 Design of inerter

In this paper, the inerter-based devices are tuned to supress the resonance of the first mode of vibration. A rotational flywheel was used to create an inerter. This concept is based on the flywheel inerter proposed by John and Wagg [37]. However, instead of using living-hinge, the flywheel inerter used in this experiment uses a linear guide to convert the translational motion from the structure into the rotational motion of the flywheel.

Figure 5 shows the flywheel inerter on an experimental rig with a shaker that was used to estimate the inertance value. The centre of the flywheel is held via a fixed support and is acting as the first terminal of the inerter. The second terminal of the inerter is on the carriage at the point where the shaker is connected. The carriage is free to move along the linear guideway, and this mechanism allows

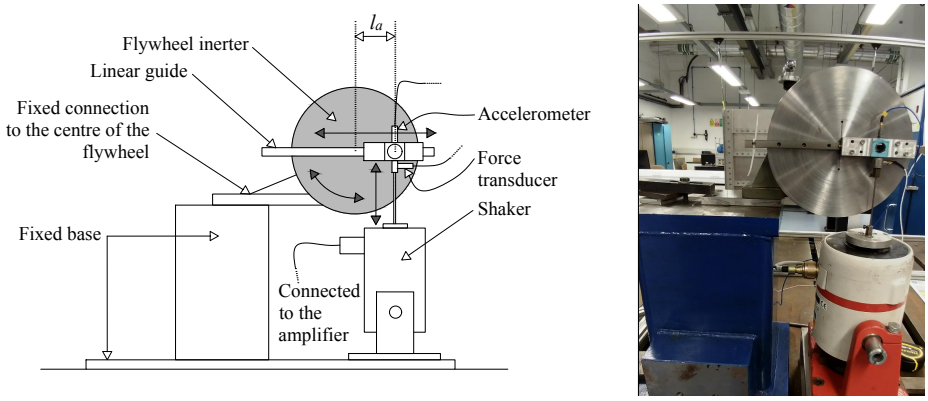

Fig. 5 Flywheel inerter experimental set-up

the flywheel to rotate during the input motion from the shaker. Note that the inertance can be adjusted by changing the distance between its two terminals, also called the lever arm, l_a. Assuming the lever arm rotation (θ) is small, the estimated inertance generated by the flywheel inerter is given by [37]

$$b_d = \frac{I}{{l_a}^2} \tag{2}$$

where I is the inertia of the flywheel.

The inerter was tested using a sinewave displacement input from the shaker with frequencies from 2-8Hz and amplitudes in the range 1-3 mm. The inertance generated is given by

$$b_d = \frac{F(t)}{a_2(t) - a_1(t)} \tag{3}$$

where $F(t)$ is the force measured by using a force transducer at the second terminal of the inerter, and $a_1(t)$ and $a_2(t)$ are the acceleration at the first and second terminals of the inerter, respectively. Note that a_1 is zero because the first terminal was fixed. Figure 6 shows the comparison between the generated inertance from the experiment and the prediction using Equation 2. As can be seen, the accuracy of the predicted inertance from Equation 2 increases with increasing lever arm, l_a. This is because with the same displacement amplitude, smaller l_a causes larger lever arm rotation θ, hence the accuracy of the small angle approximation is decreasing, and there is increasing amplitude dependency on the inertance b_d. Taking the average of the inertance across the frequency range, the relationship between the inertance and the lever arm is given in Figure 7. The results from the experiment are compared with the prediction given by the Equation 2, and the agreement is sufficient for the purposes of our current study.

3.2 Design of gel damper

The hysteretic-inerter-based device was built by connecting two gel dampers and one flywheel inerter in series. To build the gel dampers, silicone gel (Magic Power

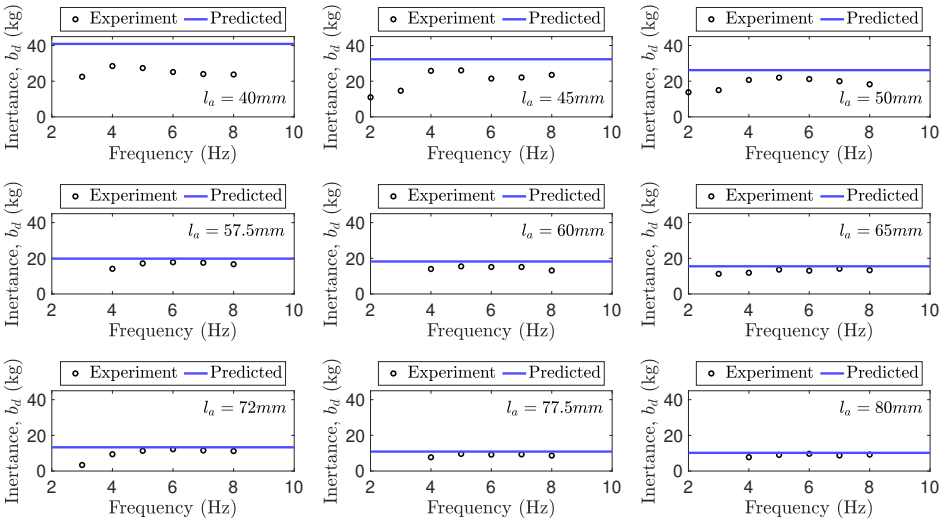

Fig. 6 Inertance across the specified frequency range, tested for selected l_a values.

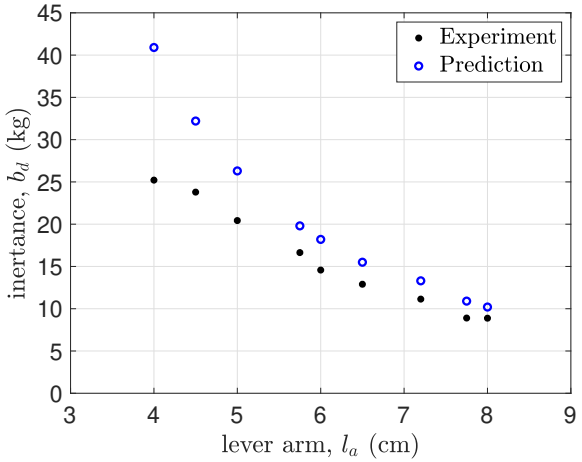

Fig. 7 Showing b_d versus l_a: Experimental results using Eq.3 compared with predicted value using Eq.2.

Gel, from Raytech) was used. This gel is normally used as an insulating gel in electrical equipment. The design of this gel damper is based on the mechanical properties given in [38]. Two gel layers were produced and placed between a sliding plate as shown in Figure 8(a). A set of characterisation tests were performed on a MTS machine using sinusoidal wave displacement input signals, $z(t)$, with a range of frequencies and amplitudes.

The forced response was measured by the force transducer on the bottom part of the damper. For each of the frequency and displacement amplitudes selected, the force versus displacement relationship shows a hysteresis loop. The area inside the loop, which represents the energy dissipated, was measured using a MATLAB script. The analytical formula for the energy dissipated by the hysteretic loop was assumed to be given by

$$\Delta W = \pi \eta k_d Z^2 \tag{4}$$

where Z is the maximum amplitude of displacement input signal $z(t)$. The loss factor η was obtained by comparing the area inside loop from the experiment and the analytical formula in Equation 4. The stiffness k_d is the slope of the hysteretic loop.

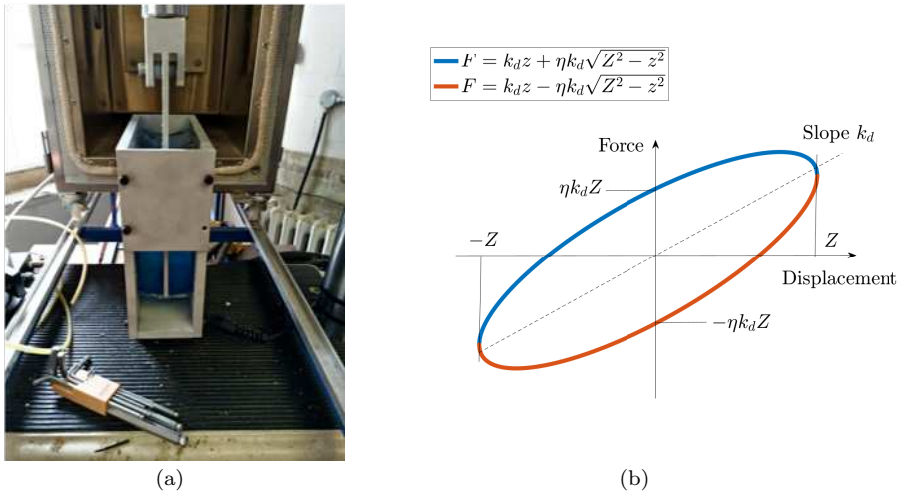

Fig. 8 Showing (a) the gel damper on a MTS test machine, (b) a schematic of the force-displacement relationship for a system with linear hysteretic damping.

It is well known that most material damping exhibits a frequency independent characteristic, meaning the energy loss per cycle represented by the area inside the hysteretic loop (e.g. Equation 4) is independent of the excitation frequency — see for example [34]. In this paper, a complex stiffness is proposed to model the hysteretic behaviour of the gel damper. The theoretical force-displacement hysteretic loop of a complex stiffness is shown in Figure 9 (a).

The comparison between this analytical model and the experiment is presented in Figure 9. As can be seen, the model gives a reasonable approximation to the real behaviour of the damper.

The tests were performed for frequency and displacement amplitude ranges of 3-8Hz and 1-12mm, respectively. The overall results indicate that the energy dissipated per cycle by the gel damper was slightly changed by the increase in the excitation frequency — an example is shown in Figure 9 (b). Moreover, there is also a dip around -0.2 mm and -1.8 mm. This is most likely due to possible imperfections in the gel, and / or imperfect bolted connections in the test machine.

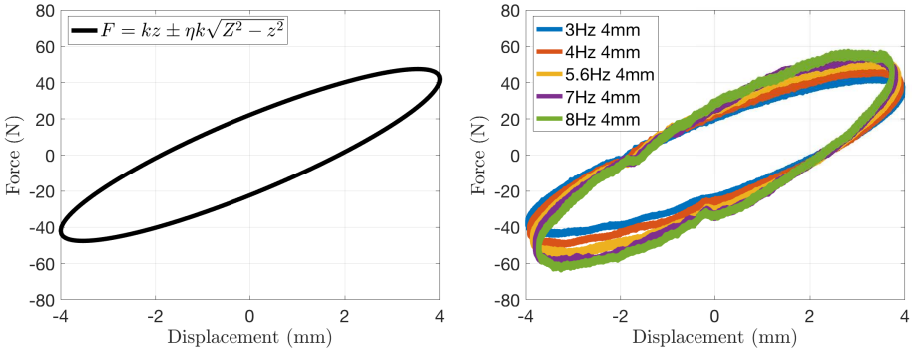

Fig. 9 Showing (a) the model of complex stiffness $F = k(1 + j\eta)z$ for displacement amplitude $Z = 4$mm, where $\eta = 0.53$Ns/mm and $k = 10.5$N/mm, and (b) data recorded from the experimental tests of one gel damper.

Table 3 Stiffness and loss factor properties of two gel dampers

Frequency (Hz)	Stiffness, k_d (N/m)		Loss factor, η	
	Experiment	Numerical	Experiment	Numerical
3	19145.72		0.46	
4	19250.00		0.52	
5.6	20958.97	21000	0.55	0.53
7	22162.16		0.57	
8	23603.21		0.57	

Theoretically the energy dissipated by the linear hysteretic damping is independent of the excitation frequency. However, despite this (relatively small) discrepancy, the area inside the loop does change (approximately) in proportion to the ratio of the square of excitation amplitude. This validates the assumed theoretically model given by Equation 4. Taking the average of the experimental results, the obtained stiffness and loss factor of the numerical model for the two gel dampers are given in Table 3.

3.3 Design of the experimental viscous-like damper

To build an experimental inerter-based device that had viscous damping type behaviour was non-trivial. The damping value of the damper needs to be selected within quite a small range in order to give the appropriate tuned device behaviour. As a result, it was decided to use eddy current dampers in order to produce a viscous-like damping effect.

Eddy current dampers produce an electromagnetic damping force proportional to the velocity of the conductor, therefore the dampers act in a very similar way to an idealised viscous damper [39]. The dampers are made of permanent magnets as shown in Figure 10(a). In the inerter-based device, the damping forces are generated by the relative motion between the permanent magnets and two aluminium sliding plates connected to two springs as shown in Figure 10(b) and 10(c). To

provide a sufficient amount of damping, a total of 632, 10×10×10mm neodymium magnets were used and arranged in a Halbach configuration. The dampers were

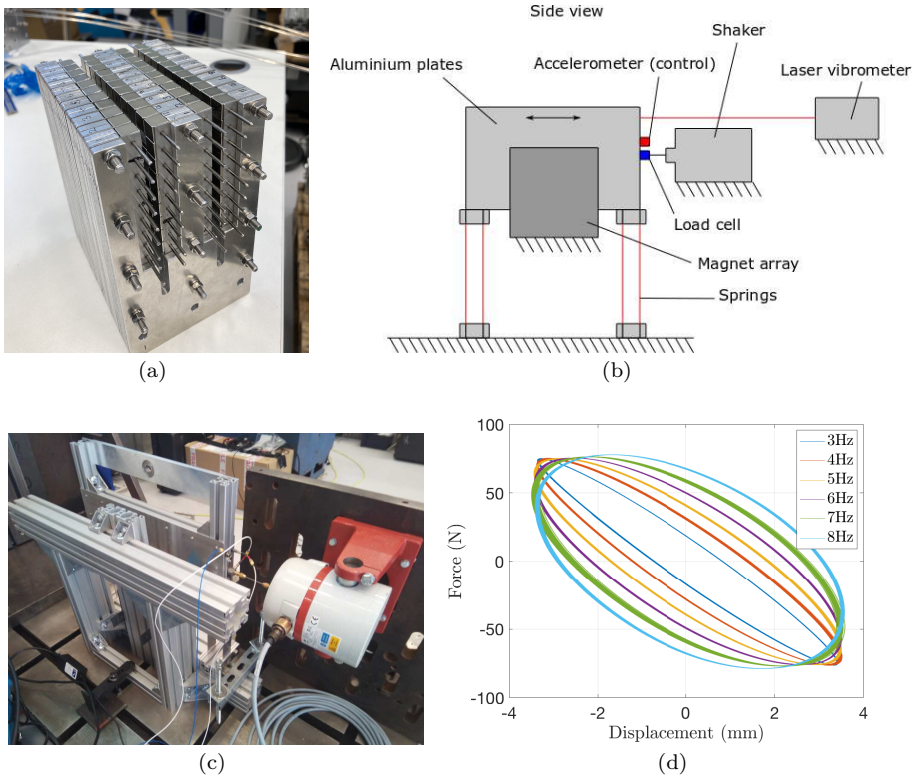

Fig. 10 Viscous-like dampers, showing (a) one block of magnetic damper consisting of several damper forks, (b) a detailed figure of the test rig, (c) a photograph of the test rig, and (d) force versus displacement hysteretic loops obtained from the characterisation tests of the magnetic dampers with a displacement amplitude of 3.5mm

firstly tested on an experimental rig shown in Figure 10(b) and 10(c) to obtain the viscous damping coefficient and the stiffness of the springs. From the obtained hysteretic loops shown in Figure 10(d), the viscous damping coefficient c_d and stiffness of the four springs k_d were identified as 0.32×10^3 Ns/m and 21400 N/m, respectively. These values were identified by first calculating the area inside the loops (which is equivalent to the energy dissipated ΔW). Then c_d was calculated using Equation 4 where ηk_d has been replaced by $c_d\omega$, hence

$$c_d = \frac{\Delta W}{\pi \omega Z^2} \tag{5}$$

where ω is the frequency of the harmonic input signal. Finally k_d was estimated by calculating the slope of the hysteretic loops.

4 Shake-table experimental tests

4.1 Experiments with the hysteretic-inerter-based system

The hysteretic-inerter-based system was built by combining the flywheel inerter and the gel dampers (described in Section 3) in series, as shown in Figure 11(b). The three-storey structure was mounted on the shake table with the hysteretic-inerter-based device installed, as shown in Figure 11(a).

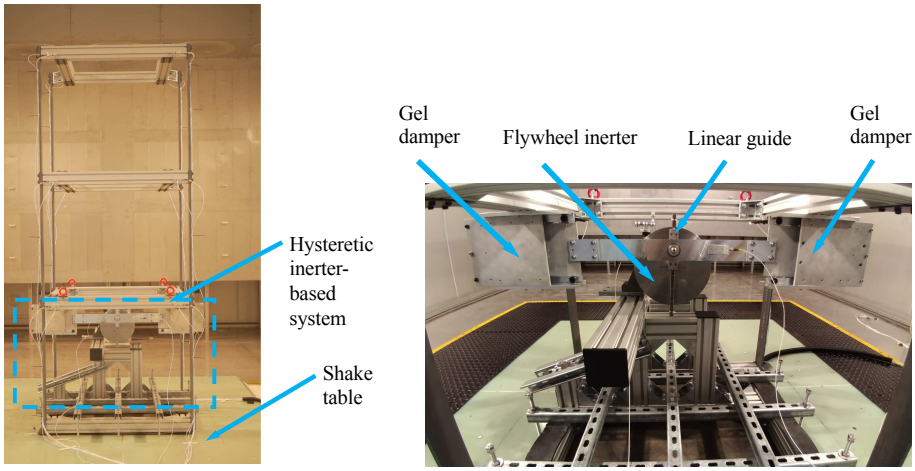

Fig. 11 Experimental three-storey structure showing: (a) the three-storey structure with a grounded hysteretic-inerter-based system, and (b) a close up of the hysteretic-inerter-based system.

Figure 11(b) shows the detailed parts of the hysteretic-inerter-based system. The first terminal of the inerter was fixed to a stiff frame which was fixed to the shake table. The second terminal of the inerter was connected to the dampers through an aluminium beam that was fixed to the middle plates between the two gel layers. The flywheel inerter was supported at its centre via a joint that was designed to allow the flywheel to be moved up and down. This mechanism makes it possible for the inertance to be adjusted by changing the distance between its two terminals before the experiment started.

In the first part of the experiment, the structure was equipped with only the two gel dampers without the inerter. One end of the hysteretic-damper is connected to the the first storey of the structure and the other end is grounded. This test was to verify the damping and stiffness properties of the gel dampers. The results of this experiment is presented in Figure 12(a). Two models are proposed and compared with the test result: (1) hysteretic damping represented by a complex stiffness; (2) viscous damping. The viscous damping coefficient is obtained via the equivalent viscous damping $c_d = \eta k_d/\omega_n$, where η and k_d are obtained from the experiment

in Section 3.2 and ω_n is the first natural frequency of the host structure. From

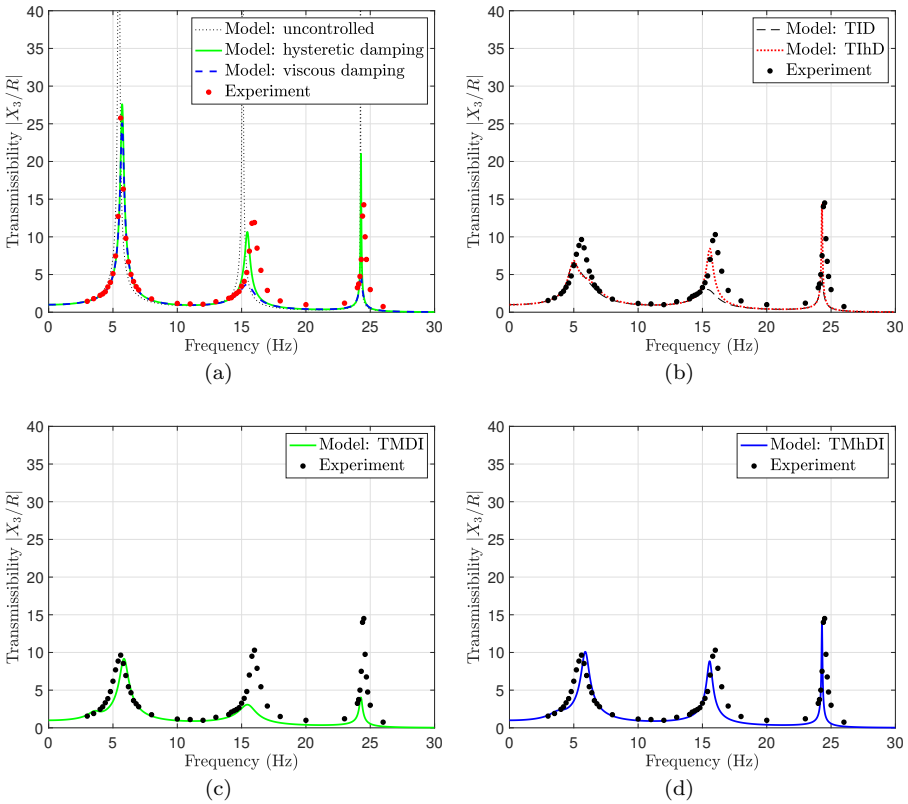

Fig. 12 Results of the three-storey structure with the inerter-based device tuned to supress the first resonance. Here showing the top floor transmissibility for: (a) the gel damper only (no inerter), (b) the full hysteretic-inerter-based system compared to the TID and TIhD models, (c) the full hysteretic-inerter-based system compared to the TMDI model, and (d) the full hysteretic-inerter-based system compared to the TMhDI model.

Figure 12(a) it is clear that the hysteretic damping model has a good agreement with the experimental test results across all tested frequencies. This implies that, (as also discussed in Section 3.2) the gel dampers exhibit linear hysteretic damping rather than viscous, and a complex stiffness model is a good representation of the dampers in this case.

In the second part of the experiment, the structure was equipped with a hysteretic-inerter-based system consisting of the two gel dampers connected in series to a flywheel inerter as shown in Figure 11(b). This device was installed between the first storey of the structure and the shake table as shown in Figure 11(a). The test result and its comparison with the four proposed analytical models is presented in Figure 12(b),12(c) and 12(d). The parameters of the numerical models are given in Table 4.

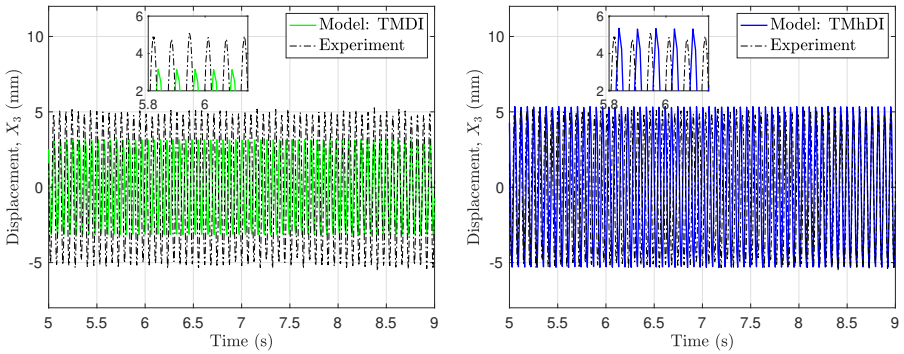

Fig. 13 Results of the three-storey structure with the inerter-based device tuned to supress the first resonance. Here showing top floor displacement at steady state with a hysteretic-inerter-based system compared to (a) the TMDI model, and (b) the TMhDI model. The excitation frequency is 15.4Hz and the base displacement amplitude is 1mm.

Table 4 Parameters of the numerical models in Figure 12

Numerical model	b_d (kg)	c_d (Ns/m)	k_d (N/m)	η	m_d (kg)
TID	18	340.65	21000	-	-
TIhD	18	-	21000	0.53	-
TMDI	18	340.65	21000	-	16
TMhDI	18	-	21000	0.53	16

It is clear from Figure 12(b) that around the first resonance neither the TIhD and TID models are in very good agreement with the experiment. This suggests that the mass of the flywheel m_d cannot be neglected in the model. The TMDI model in Figure 12(c) does show an improvement around the first resonance because the m_d value of 16kg is included (which is the self-weight of the flywheel inerter system). But the TMDI model also shows much less agreement around the second and third resonances compared to the experiment and the TIhD model. This suggests that the hysteretic damping model of the gel dampers must be treated in its original form and cannot be converted to a viscous damping via an equivalent viscous damping. As a result, the model which shows the best match to the experimental results is the TMhDI model in Figure 12(d).

A further comparison is also presented in the time domain shown in Figure 13. A frequency of 15.4Hz (around the second resonance) is chosen to highlight the difference between the TMDI and TMhDI models. The time domain analysis method for hysteretic-inerter-based dampers proposed in [35] is adopted to plot the time response of the structure with the TMhDI model. It can be seen in this figure that the TMhDI model gives a more accurate approximation to the experimental result. As also shown in Figure 12(d), the amplitude of the displacement response from the experiment is 4.9mm. Compared to the TMDI model which has amplitude of 3.06mm, the TMhDI model provides better approximation with the amplitude of 5.2mm.

4.2 Experiment with a viscous-inerter-based system

The same three-storey structure previously described was used in this experiment, as shown in Figure 14(a). However, the inerter-based system was now built by combining the flywheel inerter with the magnetic dampers and springs to provide a viscous-inerter-based system, as shown in Figure 14(b).

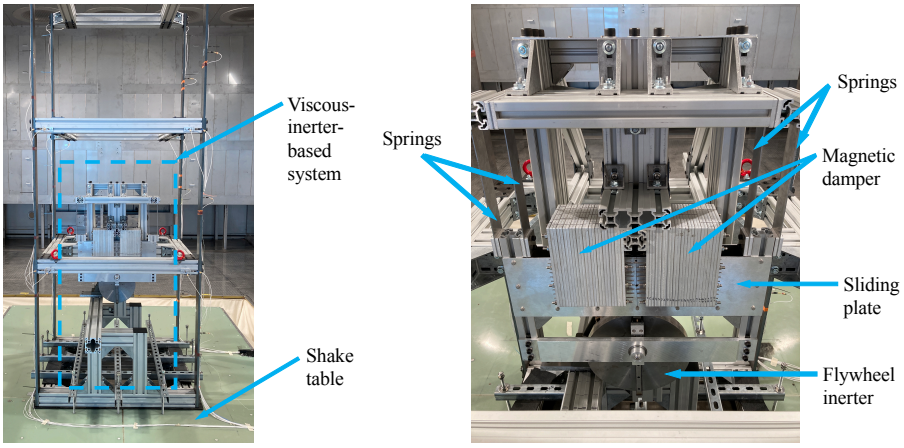

Fig. 14 Experimental three-storey structure showing: (a) the three-storey structure with a grounded viscous-inerter-based system, and (b) a close up of viscous-inerter-based system.

Similar to the previous test, there were two parts to this experiment. In the first part, the structure was equipped with only the two blocks of magnetic dampers without the inerter. This test is to verify the viscous damping coefficient of the magnetic dampers and the stiffness of the springs obtained from the characterisation test in Section 3.3. The results of this first part of the experiment are presented in Figure 15(a). It is clear from Figure 15(a) that the viscous damping model using the properties obtained from the characterisation test in Section 3.3 is in good agreement with the experimental results. From this figure, it also can be concluded that the damper does not exhibit linear hysteretic damping due to the frequency dependancy of the obtained results.

In the second part of the experiment, the 3-storey structure was equipped with a viscous-inerter-based system installed between the first storey of the structure and the table as shown in Figure 14(a). The result from the experiment was compared with the four proposed models as shown in Figure 15(b), 15(c) and 15(d). The parameters of the numerical models are given in Table 5.

As can be seen from Figure 15(b), it is clear that the first resonance of both the TIhD and TID models are not in a good agreement with the experimental data. This suggests that the mass of the flywheel m_d cannot be neglected in the model. The TMhDI model in Figure 15(d) shows a higher response around the second and third resonances compared to the experiment, and would not be expected to fit

the data, as the damping is not hysteretic. On the other hand, the TMDI model in Figure 15(c) does accurately capture the physical behaviour of the structural system equipped with the proposed viscous-inerter-based system.

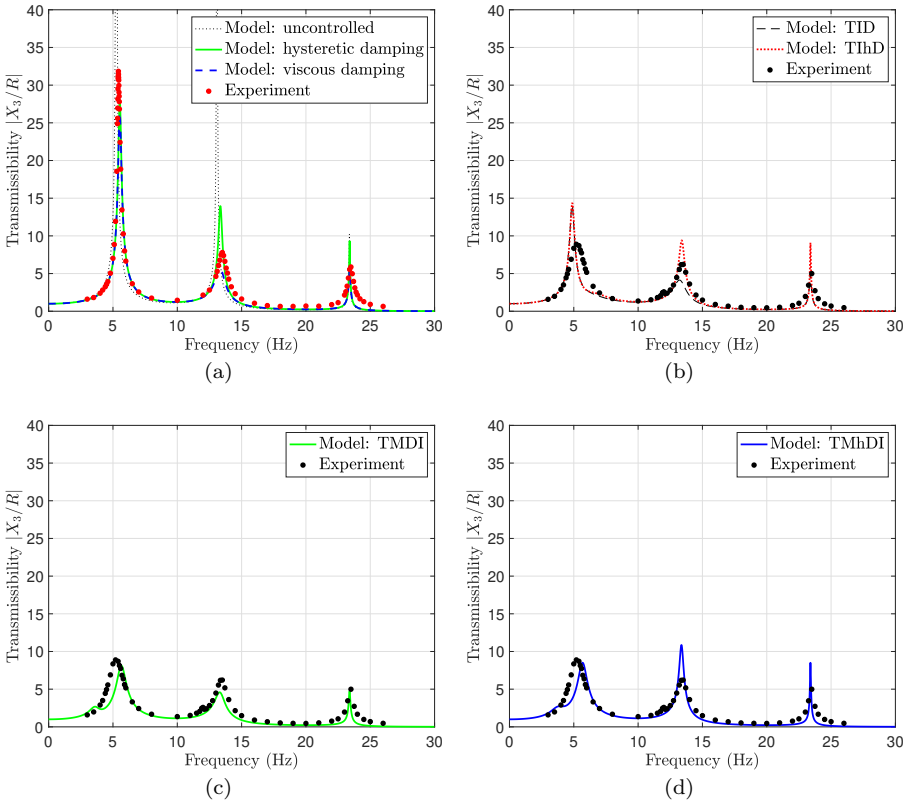

Fig. 15 Results of the three-storey structure with the inerter-based device tuned to supress the first resonance. Here showing the top floor transmissibility for: (a) the magnetic viscous-like dampers only (no inerter), (b) the viscous-inerter-based system compared to the TID and TIhD models, (c) the viscous-inerter-based system compared to the TMDI model, and (d) with the viscous-inerter-based system compared to the TMhDI model.

Table 5 Parameters of the numerical models in Figure 15

Numerical model	b_d (kg)	c_d (Ns/m)	k_d (N/m)	η	m_d (kg)
TID	15	320	21400	-	-
TIhD	15	-	21400	0.50	-
TMDI	15	320	21400	-	16
TMhDI	15	-	21400	0.50	16

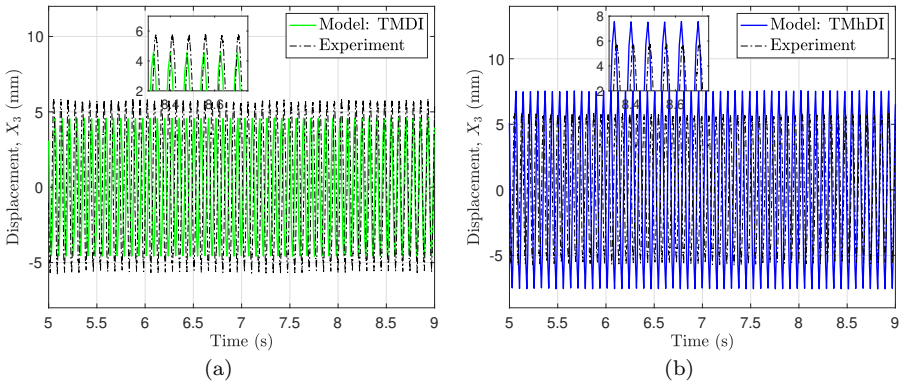

Fig. 16 Results of the three-storey structure with the inerter-based device tuned to supress the first resonance. Here showing top floor displacement at steady state with a viscous-inerter-based system compared to: (a) the TMDI model, and (b) the TMhDI model. The excitation frequency is 13.2Hz and the base displacement amplitude is 1mm.

Furthermore, the comparison is also presented in the time domain shown in Figure 16. A frequency of 13.2Hz (around the second resonance) is selected to highlight the difference between the TMDI and TMhDI models. It can be seen in this figure that the TMDI model gives a more accurate approximation to the experimental result. As also shown in Figure 15(d), the amplitude of the displacement response from the experiment is 5.7mm. Compared to the TMhDI model which has amplitude of 7.50mm, the TMDI model provides better approximation with the amplitude of 4.4mm.

It should be noted that the parameters of the numerical models in Table 4 and 5 are deliberately chosen not to be exactly the optimum 'tuned' values for suppressing the first resonance. Instead, these parameters are selected to match the real parameters of the physical devices described in Section 3. Initially, the design of the flywheel inerter, gel dampers and eddy current dampers were focused on obtaining optimal parameters for suppressing the first resonance based on fixed-point theory [8]. However, due to the physical constraints of the manufacturing processes, the obtained physical properties of these devices are not exactly optimum. However, they are as close to optimum as it was physically possible to manufacture. Therefore, there is not a 'split peak' in the targeted first resonance in the results presented in Figure 12 and 15, (b), (c) and (d).

5 Discussion

In this paper experimental results are presented from shake table tests on a scaled multi-storey structure with inerter-based devices that have both viscous and hysteretic damping characteristics. The inerter-based devices were designed to suppress vibration amplitudes at the first resonant peak. This gave a significant vibration mitigation effect, but due to constraints in the manufacturing process, the 'split peak' typically seen in purely numerical studies was not possible to obtain in the experiments.

Despite this, the results of the modelling give very good agreement with the experimental results. In particular, for the inerter-based device with hysteretic damper, the TMhDI model gave the best fit to the experimental data, as shown in Figure 12(d). For the inerter-based device with viscous damper, the TMDI model gave the best fit to the experimental data, as shown in Figure 15(c).

In absolute terms, the inerter-based device with viscous damping performs significantly better than the device with hysteretic damping in terms of reducing the amplitude over all the three resonance peaks. This can be observed by comparing Figures 12(d) and 15(c). The potential problem with this is that viscous damping is an idealisation, and is not always possible to implement in practice. So for systems where the damping behaviour may be closer to hysteretic this should be taken into consideration during the design of the system.

This has been noted before in terms of a comparison of the numerical models, and discussed in detail by [35]. The results presented here provide experimental validation of this phenomena. Furthermore, in [35] it was shown that the hysteretic-inerter-based system cannot be effectively modelled using an equivalent viscous damping approach. Therefore, the linear hysteretic damping must be treated in its original form when performing both frequency and time domain analyses. In this regard, the complex damping model has been shown in [35] to be a good representation of the linear hysteretic damping of the hysteretic-inerter-based system when comparing the analytical frequency-domain and time-domain results.

This confirms two important modelling considerations: (1) the mass of the flywheel inerter m_d cannot be neglected in either case; (2) the linear hysteretic damping cannot be approximated (across a range of frequencies) by an equivalent viscous damping, and it should therefore be modelled as a complex stiffness, if the multi-mode behaviour is required to be accurately modelled.

6 Conclusions

In this paper, for the first time, experimental results have been presented from shake-table experiments of a multi-storey structure equipped with inerter-based devices with hysteretic and viscous damping. The rationale was to obtain sufficient experimental data in order to validate mathematical models typically used to model the dynamics of inerter-based devices that were tuned to supress vibrations of the first resonance. The type of damping used in such models is very important, as it leads to significant differences in the resonant behaviour of the structure being controlled.

Overall, the experimental results presented in this paper demonstrate (within the limitations of the type of system and parameter ranges considered) that the TMDI model is the best for modelling viscous-inerter-based systems. However, for hysteretic-inerter-based systems the TMhDI model needs to be used to accurately predict the physical behaviour.

In terms of overall behaviour, the viscous-inerter-based system performs better than the hysteretic-inerter-based system, particularly in terms of mitigating the vibration of the second and third resonance peaks.

Acknowledgements The authors would like to thank Mr Mathew J Hall and Mr Michael J Dutchman for their help on the design, manufacturing and testing of the inerter, gel and magnetic dampers.

Declarations

The first author is funded by the Indonesia endowment fund for education (LPDP). This research also made use of The Laboratory for Verification and Validation (LVV) which was funded by the EPSRC (grant numbers EP/R006768/1 and EP/N010884/1), the European Regional Development Fund (ERDF) and the University of Sheffield. The authors declare that they have no conflict of interest.

References

1. Smith, M. C. (2002). Synthesis of mechanical networks: the inerter. IEEE Transactions on automatic control, 47(10), 1648-1662.
2. Okumura A. (2007). Japan Patent Koukai. H09-177875.
3. Ikago, K., Saito, K., Inoue, N. (2012). Seismic control of single-degree-of-freedom structure using tuned viscous mass damper. Earthquake Engineering & Structural Dynamics, 41(3), 453-474.
4. Smith MC. (2001). Force-controlling mechanical device. US Patent 7,316,303.
5. Wang, F. C., Hong, M. F., Lin, T. C. (2011). Designing and testing a hydraulic inerter. Proceedings of the Institution of Mechanical Engineers, Part C: Journal of Mechanical Engineering Science, 225(1), 66-72.
6. Wagg, D. J. (2021). A review of the mechanical inerter: historical context, physical realisations and nonlinear applications. Nonlinear Dynamics, 104, 13–34.
7. Saito, K., Sugimura, Y., Nakaminami, S., Kida, H., Inoue, N. (2008). Vibration tests of 1-storey response control system using inertial mass and optimized soft spring and viscous element. Journal of Structural Engineering, 54, 623-634.
8. Lazar, I. F., Neild, S. A., Wagg, D. J. (2014). Using an inerter-based device for structural vibration suppression. Earthquake Engineering & Structural Dynamics, 43(8), 1129-1147.
9. Marian, L., Giaralis, A. (2014). Optimal design of a novel tuned mass-damper–inerter (TMDI) passive vibration control configuration for stochastically support-excited structural systems. Probabilistic Engineering Mechanics, 38, 156-164.
10. Sugimura, Y., Goto, W., Tanizawa, H., Saito, K., Nimomiya, T. (2012). Response control effect of steel building structure using tuned viscous mass damper. In Proceedings of the 15th world conference on earthquake engineering (pp. 24-28).
11. Deastra, P., Wagg, D. J., Sims, N. D. (2019). The realisation of an inerter-based system using fluid inerter. In Dynamics of Civil Structures, Volume 2 (pp. 127-134). Springer, Cham.
12. Pietrosanti, D., De Angelis, M., Basili, M. (2017). Optimal design and performance evaluation of systems with Tuned Mass Damper Inerter (TMDI). Earthquake Engineering & Structural Dynamics, 46(8), 1367-1388.
13. De Domenico, D., Ricciardi, G. (2018). An enhanced base isolation system equipped with optimal tuned mass damper inerter (TMDI). Earthquake engineering & structural dynamics, 47(5), 1169-1192.
14. Pietrosanti, D., De Angelis, M. and Basili, M., 2020. A generalized 2-DOF model for optimal design of MDOF structures controlled by Tuned Mass Damper Inerter (TMDI). International Journal of Mechanical Sciences, 185, p.105849.
15. Papageorgiou, C., Houghton, N. E., Smith, M. C. (2009). Experimental testing and analysis of inerter devices. Journal of dynamic systems, measurement, and control, 131(1).
16. Giaralis, A., Petrini, F. (2017). Wind-induced vibration mitigation in tall buildings using the tuned mass-damper-inerter. Journal of Structural Engineering, 143(9), 04017127.
17. Dai, J., Xu, Z. D., Gai, P. P. (2019). Tuned mass-damper-inerter control of wind-induced vibration of flexible structures based on inerter location. Engineering Structures, 199, 109585.
18. Radu, A., Lazar, I. F., Neild, S. A. (2019). Performance-based seismic design of tuned inerter dampers. Structural Control and Health Monitoring, 26(5), e2346.

19. De Domenico, D., Ricciardi, G. (2018). Optimal design and seismic performance of tuned mass damper inerter (TMDI) for structures with nonlinear base isolation systems. Earthquake engineering & structural dynamics, 47(12), 2539-2560.
20. Deastra, P., Wagg, D. J., Sims, N. D. (2018). The effect of a tuned-inerter-damper on the seismic response of base-isolated structures. In 16th European Conference on Earthquake Engineering (pp. 18-21).
21. Deastra, P., Wagg, D. J., Sims, N. D. (2021). Using a Tuned-Inerto-Viscous-Hysteretic-Damper (TIVhD) for vibration suppression in multi-storey building structures. In IOP Conference Series: Earth and Environmental Science (Vol. 708, No. 1, p. 012012). IOP Publishing.
22. Giaralis, A., Taflanidis, A. A. (2018). Optimal tuned mass-damper-inerter (TMDI) design for seismically excited MDOF structures with model uncertainties based on reliability criteria. Structural Control and Health Monitoring, 25(2), e2082.
23. Ariga, T., Kanno, Y., Takewaki, I. (2006). Resonant behaviour of base-isolated high-rise buildings under long-period ground motions. The Structural Design of Tall and Special Buildings, 15(3), 325-338.
24. Kamae, K., Kawabe, H., Irikura, K. (2004). Strong ground motion prediction for huge subduction earthquakes using a characterized source model and several simulation techniques. In Proceedings of the 13th WCEE.
25. Tsai, H. C. (1995). The effect of tuned-mass dampers on the seismic response of base-isolated structures. International journal of solids and structures, 32(8-9), 1195-1210.
26. De Domenico, D., Deastra, P., Ricciardi, G., Sims, N. D., Wagg, D. J. (2019). Novel fluid inerter based tuned mass dampers for optimised structural control of base-isolated buildings. Journal of the Franklin Institute, 356(14), 7626-7649.
27. Saitoh, M. (2012). On the performance of gyro-mass devices for displacement mitigation in base isolation systems. Structural Control and Health Monitoring, 19(2), 246-259.
28. Hessabi, R. M., Mercan, O., Ozturk, B. (2017). Exploring the effects of tuned mass dampers on the seismic performance of structures with nonlinear base isolation systems. Earthquakes and Structures, 12(3), 285-296.
29. De Angelis, M., Giaralis, A., Petrini, F. and Pietrosanti, D., 2019. Optimal tuning and assessment of inertial dampers with grounded inerter for vibration control of seismically excited base-isolated systems. Engineering Structures, 196, p.109250.
30. Brzeski, P., Lazarek, M., Perlikowski, P. (2017). Experimental study of the novel tuned mass damper with inerter which enables changes of inertance. Journal of Sound and Vibration, 404, 47-57.
31. Gonzalez-Buelga, A., Lazar, I. F., Jiang, J. Z., Neild, S. A., Inman, D. J. (2017). Assessing the effect of nonlinearities on the performance of a tuned inerter damper. Structural Control and Health Monitoring, 24(3), e1879.
32. Pietrosanti, D., De Angelis, M., Giaralis, A. (2020). Experimental study and numerical modeling of nonlinear dynamic response of SDOF system equipped with tuned mass damper inerter (TMDI) tested on shaking table under harmonic excitation. International Journal of Mechanical Sciences, 184, 105762.
33. Pietrosanti, D., De Angelis, M. and Giaralis, A., 2021. Experimental seismic performance assessment and numerical modelling of nonlinear inerter vibration absorber (IVA)-equipped base isolated structures tested on shaking table. Earthquake Engineering & Structural Dynamics, 50(10), 2732-2753.
34. C. F. Beards. (1996). Structural Vibrations: Analysis and Damping. Halsted Press.
35. Deastra, P., Wagg, D., Sims, N., Akbar, M. (2020). Tuned inerter dampers with linear hysteretic damping. Earthquake Engineering & Structural Dynamics, 49(12), 1216-1235.
36. Inaudi, J. A., Makris, N. (1996). Time-domain analysis of linear hysteretic damping. Earthquake engineering & structural dynamics, 25(6), 529-545.
37. John, E. D., Wagg, D. J. (2019). Design and testing of a frictionless mechanical inerter device using living-hinges. Journal of the Franklin Institute, 356(14), 7650-7668.
38. Almagirby, A. A. (2016). Understanding Vibration Transmitted to the Human Finger (Doctoral dissertation, University of Sheffield).
39. Mazza, F., Labernarda, R. (2020). Magnetic damped links to reduce internal seismic pounding in base-isolated buildings. Bulletin of Earthquake Engineering, 18(15), 6795-6824.